Magnetic field melting of the charge-ordered state of $La_{1/2}Ca_{1/2}MnO_3$: A local structure perspective

T. A. Tyson,[1] M. Deleon,[1] M. Croft,[2] V. G. Harris,[3,*] C.-C. Kao,[4] J. Kirkland,[3] and S-W. Cheong[2]
[1]*Department of Physics, New Jersey Institute of Technology, Newark, New Jersey 07102, USA*
[2]*Department of Physics and Astronomy, Rutgers University, Piscataway, New Jersey 08854, USA*
[3]*Materials Physics Branch, Naval Research Laboratory, Washington DC 20375, USA*
[4]*Brookhaven National Laboratory, Upton, Long Island, New York 11973, USA*
(Received 9 June 2003; revised manuscript received 24 March 2004; published 15 July 2004)

The local structure about the Mn site in the half-doped system $La_{1/2}Ca_{1/2}MnO_3$ was measured in magnetic fields up 10 T to probe the melting of the charge-ordered state. Examination of the Mn-O and Mn-Mn correlations reveals three distinct regions in the structure-field diagram. A broad region with weak field dependence (mainly antiferromagnetic phase below 7.5 T), a narrow-mixed phase region near ~8.5 T and a high-field ferromagnetic phase region with strong field-structure coupling are found. At high field the Mn-O radial distribution becomes Gaussian and the Mn-Mn correlations are enhanced—consistent with the dominance of a ferromagnetic phase. Comparison of the structural measurements with transport and magnetization measurements suggests that the exponential changes in resistivity in the first region are dominated by the reordering of the moments on the Mn sites from CE type antiferromagnetic to ferromagnetic order with only a weak change in the local distortions of the MnO_6 octahedra.

DOI: 10.1103/PhysRevB.70.024410 PACS number(s): 78.70.Dm, 61.10.Ht, 75.47.Lx, 87.64.Gb

I. INTRODUCTION

The manganite system [$R_{1-x}A_xMnO_3$, where A is a divalent cation (such as Ca, Sr, or Ba) and R is a trivalent rare-earth metal] has intriguing properties manifested by complex phase diagrams which can be tuned by doping, internal and external pressure and electric and magnetic fields.[1–3] As a function of these parameters and x (doping level), the system can be forced between metallic and insulating regions. For the classic $La_{1-x}Ca_xMnO_3$ system, the reference state ($x=0$) is an antiferromagnetic insulator. Ca doping produces a ferromagnetic conducting system for $x\sim0.2-\sim0.5$ and for $x>0.5$ antiferromagnetic insulating phases are found. These materials are rich in intriguing phenomena and are an excellent test bed for studies of systems in which electron-electron and electron phonon interactions cannot be neglected.[4]

The half-dopped system $La_{1/2}Ca_{1/2}MnO_3$ is at the boundary of the ferromagnetic and charge-ordered (CO) insulating region of the phase diagram. These systems are characterized by the onset of ferromagnetic ordering (dominated by the double exchange) followed by a significant loss of bulk magnetization at lower temperature where superexchange dominates. The delicate balance between superexchange and double exchange can be shifted by application magnetic fields[5–14] and Mn site doping.[15] In $La_{1/2}Ca_{1/2}MnO_3$, neutron diffraction measurements found evidence for distinct structural phases corresponding to ferromagnetic and antiferromagnetic regions coexisting at low temperature.[16,17] Cooling in high magnetic field is found to stabilize the ferromagnetic phase and reverse the volume ratios of the two phases.[16,18]

The coupling to magnetic field suggests very closely lying energy states of different magnetic structures. Indeed, in $La_{1/2}Ca_{1/2}MnO_3$, the coexistence of mixed phases of insulating and metallic region has been found to be a common feature of manganites and other strongly correlated systems due to the small atomic changes required to move from one phase to another.[19,20] Intertwined ferromagnetic (with full saturation magnetic moments per Mn site) and antiferromagnetic regions have been observed on a nanoscale.[20]

In order to explore the nature of the magnetic field induced melting of the CO state in $La_{1/2}Ca_{1/2}MnO_3$, a local structural perspective is needed. X-ray absorption spectroscopy enables one to measure the average structure about a specific atom unbiased by the need to impose a long-rang structure. This approach enabled studies of the local distortions in the MnO_6 octahedra near $x\sim0.3$ in $La_{1-x}Ca_xMnO_3$ which revealed the loss of the Jahn Teller (JT) distortions on going into the low-temperature metallic phase.[21]

The $La_{1/2}Ca_{1/2}MnO_3$ system is characterized by the onset of ferromagnetism near 225 K (T_C) followed by a near collapse of the net magnetization below $T_N\sim155$ K. The low-temperature phase has been described as a charge (Mn^{3+} and Mn^{4+}) and orbital ordered state. In order to understand the structural details of the magnetic field melting of the CO state, we have performed magnetic field dependent x-ray absorption measurements. We have found that the Debye-Waller (DW) factor for the Mn-O distribution is reduced by 40% between 0 and 10 T. Examination of the Mn-O and Mn-Mn correlation reveals three distinct regions in the structure-field diagram—a broad region with weak field dependence (mainly antiferromagnetic phase below 7.5 T), a narrow-mixed phase region near ~8.5 T followed by a ferromagnetic phase region with strong field-structure coupling. The Mn-O radial distribution becomes Gaussian and the Mn-Mn correlations are enhanced in the high field region—consistent with the dominance of a ferromagnetic phase. Comparison of the structural measurements with transport and magnetization measurements suggests that the exponential changes in resistivity in the first region are dominated by

the reordering of the moments on the Mn sites from CE type antiferromagnetic to ferromagnetic order with only a weak change in the local distortions of the MnO_6 octahedra. The more rapid reduction in resistivity at high field is seen to be the result the delocalization of JT trapped electrons as the magnetic field destabilizes the local distortions.

II. EXPERIMENTAL METHODS

The polycrystalline sample of $La_{1/2}Ca_{1/2}MnO_3$ and $CaMnO_3$ were prepared by solid state reaction in air as described in Ref. 22 and extensive studies of the transport, magnetic, and zero field structural studies were presented in Ref. 23. The Néel and Curie temperatures of the samples were 155 and 225 K, respectively. X-ray absorption samples (XAFS) were prepared by grinding the sample to form a 400 mesh powder and brushing it onto scotch tape. Layers of tape were stacked to produce a uniform sample for transmission measurements with a jump $\mu t \sim 1$. A custom designed Oxford Instruments 10 T split-coil horizontal field superconducting magnet was used for the measurements.[24] All measurements reported were performed with the x-ray beam parallel to the magnetic field. Measurements with varying field were made by cooling the sample to 115 ± 0.01 K (into the charge-ordered phase) at zero magnetic field. The field was then stepped up with x-ray absorption measurements performed at each step with the magnet in persistent current mode. Temperature dependent XAFS measurements were conducted with decreasing temperatures starting at 295 K (Fig. 3).

Spectra were measured at the National Synchrotron Light Source (NSLS) at Brookhaven National Laboratory utilizing beam line X23B and a Si(111) monochromator and focusing torroidal mirror with an energy cutoff of 11 KeV were used. Spectra were taken in transmission mode using nitrogen filled ion chambers. A Mn foil reference was employed for energy calibration. The reduction of the XAFS data was performed using standard procedures.[25] Calibration was accomplished be defining the first inflection point in the spectrum of Mn metal as 6539 eV. The ionization threshold E_0 was set at 6554.5 eV based on the zero field spectrum. The photoelectron momentum is defined as $k=\sqrt{(2m/\hbar^2)(E-E_0)}$. XAFS were extracted from the spectra as the difference between the normalized spectra and an adjustable spline function fit through the post-edge region, the parameters of which were adjusted to minimize low frequency residuals in the Fourier transform below $R=0.75$ Å.[26] After comparison, two to four individual scans were averaged [see Fig. 1(a)].

Fits to the first shell Mn-O distribution were performed by Fourier transforming the XAFS data over the range $2.54 < k < 14.5$ Å^{-1} to R space.[27] The R-space fits (Fig. 2) to theoretical signals[28] based on the low-temperature structure[29] of $La_{1/2}Ca_{1/2}MnO_3$ were performed over the range $0.75 < R < 1.95$ Å assuming a cumulant expansion[30] of the radial distribution [Fig. 1(b)]. The simplest model which fit the data well consists of an amplitude reduction factor $S_0^2 = 0.7$ variable parameters R (average bond distance), σ^2 **(**the DW factor $[\langle (R-\langle R\rangle)^2\rangle$ mean squared relative displacement]

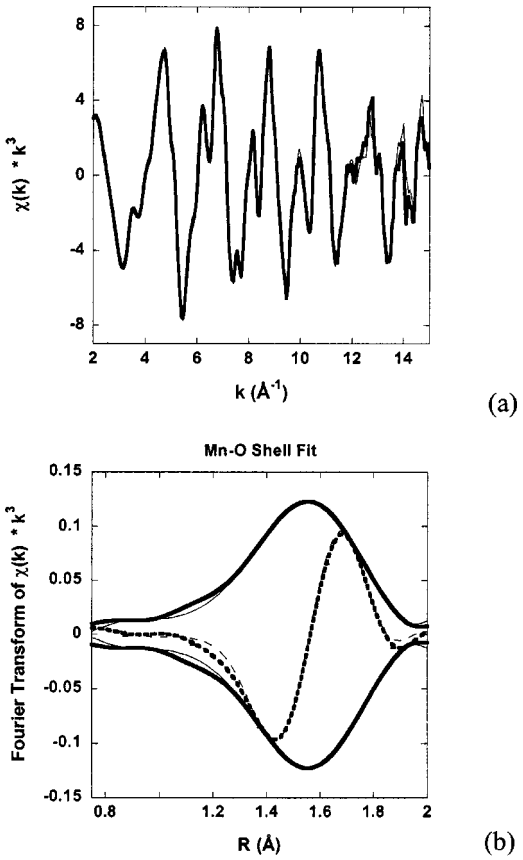

FIG. 1. (a) Extracted $La_{1/2}Ca_{1/2}MnO_3$ XAFS data for two consecutive scans at 115 K and zero field are displayed to show the level of the noise in the data. The first and second scan are displayed as thick and thin lines, respectively. (b) Typical fit to Mn-O shell over the range $0.75 < R < 1.95$ Å with thin lines corresponding to the data and thick lines corresponding to the fit. The dashed and solid lines correspond to the magnitude and imaginary parts, respectively.

representing the width of the distribution**)** and C4 [kurtosis or flatness of the distribution $\langle (R-\langle R\rangle)^4\rangle - 3\sigma^4$]. The first shell coordination number was held fixed at 6. The total number of free parameters in the fit was 3, compared to the theoretical maximum number of independent parameters $2\Delta k \Delta r/\pi + 2 = 7$.[31] Parameter errors were obtained by determining the stability of the fits with respect to changes in each parameter.

III. RESULTS AND DISCUSSION

Measurements were made at 115 K, deep within the CO ($T_N \sim 155$ K) region of this half-doped system. Fourier transform spectra (qualitatively analogous to radial distributions with the caveat that the amplitude is scattering atom dependent and the peak positions are shifted toward the origin by the phase of the atomic scattering factor) of the field-dependent XAFS data from 0 to 10 T are shown in Fig. 2 with the Mn-O, Mn-Ca/La, and Mn-Mn/Mn-O-Mn peaks labeled. Note the enhancement of Mn-O peak with increasing magnetic field. This indicates that there is a reduction of the MnO_6 octahedral distortion with field.

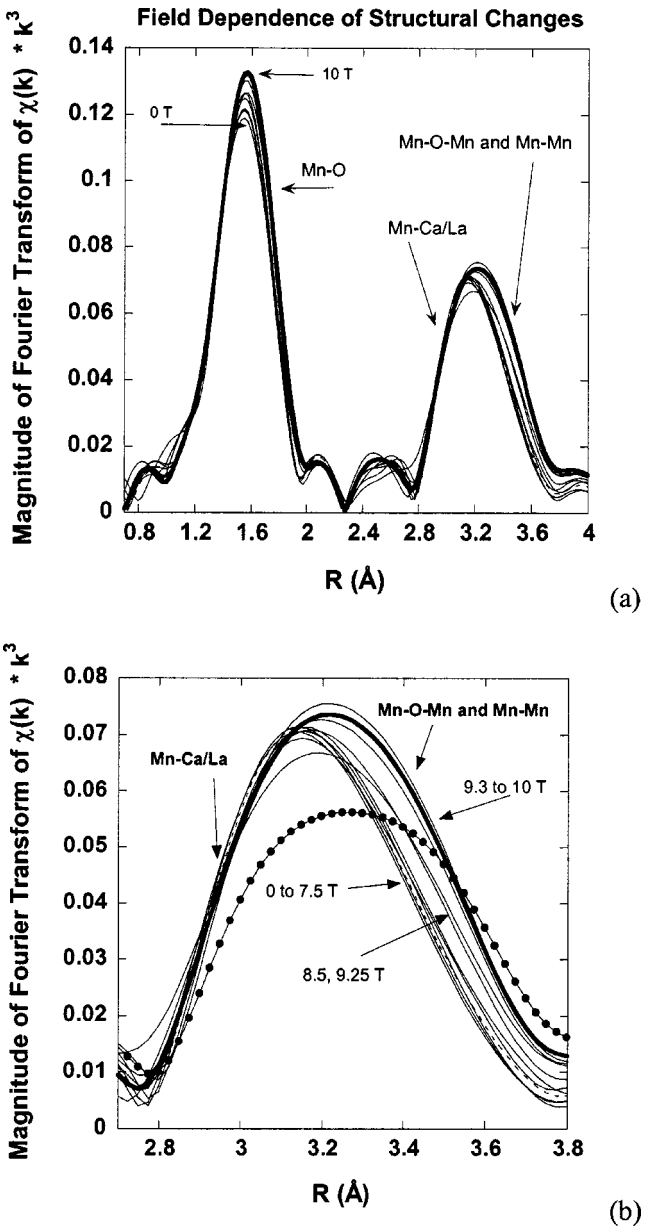

FIG. 2. (a) Fourier transfrom of the field dependent XAFS data (as in Fig. 1) over the range $2.54 < k < 14.05$ Å^{-1} with the Mn-O, Mn-Ca/La, and Mn-Mn/Mn-O-Mn peaks labeled. (b) The expanded Mn-Mn/Mn-O-Mn peak shows that three distinct structural regions exist. The zero field 295 and 115 K spectra are shown the dotted line and dashed lines, respectively.

A systematization of the trends with field can be obtained by looking at the higher order bond correlations. Note the strong enhancement of the Mn-Mn/Mn-O-Mn shoulder at high field (above 8.5 T). In Fig. 2(b) we expand the Mn-Mn/Mn-O-Mn peak to show that three distinct structural regions exist. For fields below ~7.5 T the low-temperature charge-ordered (AF) structure is maintained. Between ~8.5 and ~9.25 T a mixed-phase region exists. Above ~9.3 T, a ferromagnetic phase exists with structure similar to the high-temperature paramagnetic phase (295 K, solid dotted line).

For comparison we show the temperature-dependent zero field XAFS spectra measured on cooling (Fig. 3). There are thermal effects which enhance the amplitudes at low temperature. However, the collapse of the Mn-Mn/Mn-O-Mn feature below ~180 K (between T_C and T_N) is evident. This is the feature which is recovered in the field-dependent measurement. Hence the reduced Mn-Mn correlation signals the onset of the charge-ordered AF state. Comparison of the high-field data in Fig. 2(b) with the high-temperature data in Fig. 3(b) suggests that the gross ferromagnetic/paramagnetic state structure is recovered by application of a 10 T field at 115 K. The details of this field induced state will now be addressed.

To quantify the changes in the local structure about the Mn site we have extracted the DW factor $[\sigma^2 = \langle (R - \langle R \rangle)^2 \rangle]$ or variance of the Mn-O distribution as a function of the magnetic field (Fig. 4). The results are compared with high-field measurements of the magnetization by Xiao *et al.*[5] (We note that the difference in the magnetization measured at 108 K and our XAFS measurements at 115 K are within the size of the solid dots.) The moment at 10 T is 3.0 μ_B/Mn site and changes by only 4% between 10 and 18 T.[5] The saturation moment of 3.5 μ_B/Mn is not achieved even at these high fields. However at low temperature (below 77 K) the saturation moment is achieved over the same field region indicating the moment loss is due to thermal disorder of the moments.[5] Since the moment loss is small, we make arguments concerning the saturation limit in σ^2 (H). Note that at high field the JT distortion is strongly suppressed. The high-field values should be compared to the value $\sigma^2 = 0.00254 \pm 0.00021$ Å^2 found for $CaMnO_3$ (at 300 K) with octahedral Mn-O distances of 1.895, 1.900, and 1.903 Å.[32] The data points are labeled near the region of rapid change in amplitude. As mentioned above, the distribution of Mn-O distances in zero field is non-Gaussian and is described by one additional parameter $[C4 = \langle (R - \langle R \rangle)^4 \rangle - 3\ \sigma^4]$ characterizing the flatness (due to multiple Mn-O bond lengths). In Fig. 5 we see that at high field C4 vanishes indicating the disappearance of the JT distortion (resulting in a narrow Gaussian distribution of distances).

In Fig. 6 we show the average distance as a function of magnetic field. The average Mn-O bond distance approaches 1.96 Å, the value measured in the optimally ferromagnetic region of the $La_{1-x}Ca_xMnO_3$ phase diagram near $x = 0.33$.[33] Again the increase in bond distance above 7.5 T signals the existence of a mixed phase region occurring before transformation to the ferromagnetic phase.

In Fig. 7, we plot the DW factor (σ^2) as a function of the magnetization. One can clearly see from this figure that in the CO region that JT distortion decreases approximately linearly with the spin polarization. On crossing into the ferromagnetic metal (FMM) phase, the decrease in the distortion occurs at a rate 100 times higher than in the CO region.

The origin of the large decrease in resistivity observed in this system can be interpreted with this additional information.[5,8] The JT distortion on the Mn site traps the e_g electrons and reduces the mobile carrier density. Application of a magnetic field first polarizes (aligns) the Mn

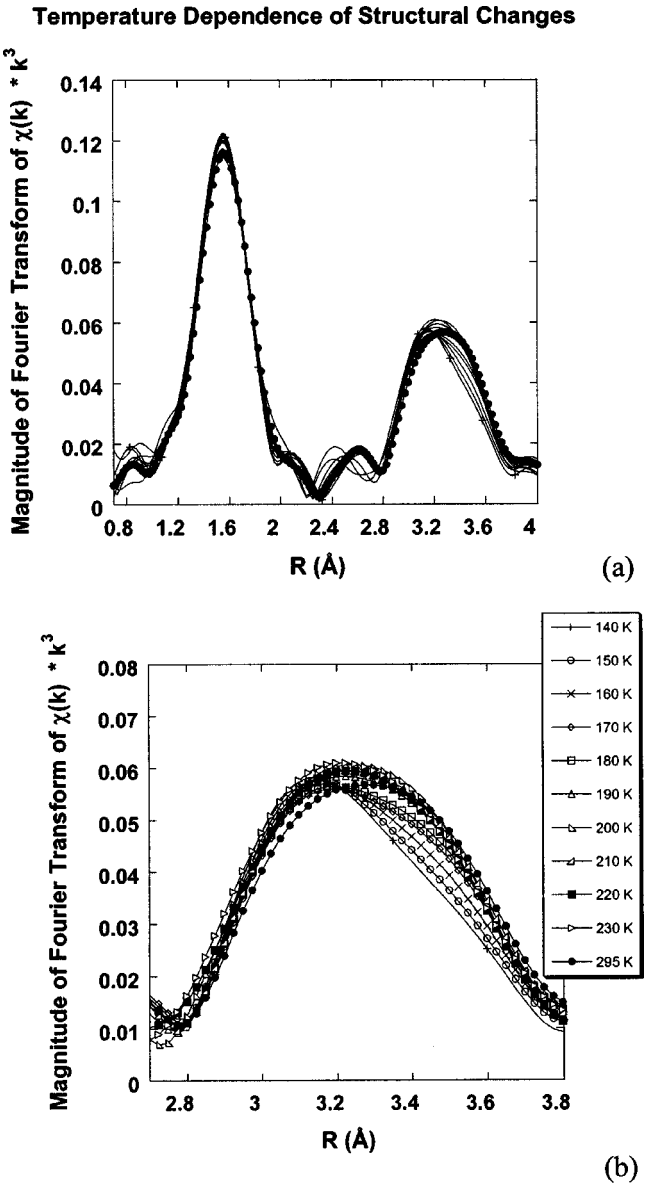

FIG. 3. Temperature-dependent data at zero field (treated in the same manner as the field-dependent measurements) are shown for comparison. In (a) the full spectra are shown. The second peak is expanded in panel (b). Note the collapse of the Mn-Mn/Mn-O-Mn peak occurs near ~180 K (between T_c and T_N). Data were transformed over the useful data range $2.54 < k < 13.18$ Å^{-1} limited by the reduction in signal to noise with increased temperature.

moments by destroying the CF AF phase leading to an exponential drop in resistivity. Application of a field beyond the first critical field then results in the collapse of the JT distortion concomitant with a change in the long-range structure further reducing the resistivity. At high field the e_g electrons become untrapped, with progressively lower binding and are able to mediate the ferromagnetic interactions between Mn sites.

We note that the reduction of the DW factor is of the order of 40% when comparing the 0 and 10 T values. This value matches well with the temperature-dependent collapse of the DW factor in the ferromagnetic phase of

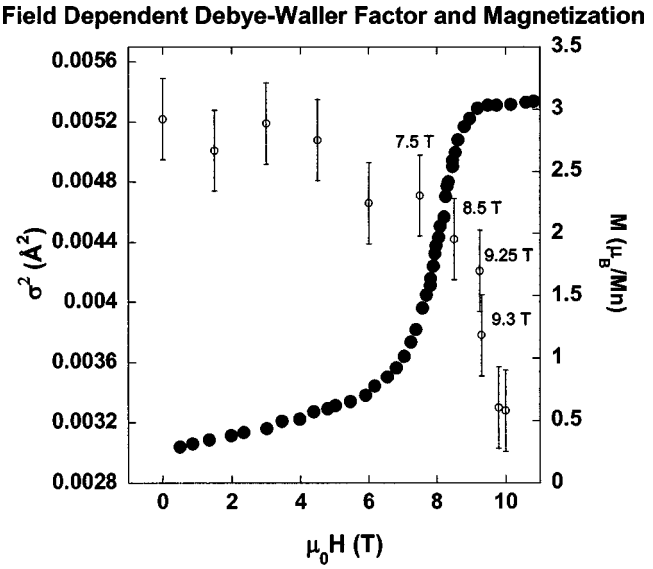

FIG. 4. The field-dependent Debye-Waller factor ($\sigma^2 = \langle (R - \langle R \rangle)^2 \rangle$, open circles) for the Mn-O bond compared with the magnetization [solid dots taken from Xiao *et al.* (Ref. 5)].

$La_{1-x}Ca_xMnO_3$ ($x \sim 0.33$) on going from the high-temperature insulating and paramagnetic state to the low-temperature ferromagnetic metallic state.[21] Two additional factors point to the complete collapse of the CO phase at high field. The strong suppression of the Debye-Waller factor in the high-field region (above 9.25 T) is characteristic of behavior found at low fields in optimally doped (ferromagnetic metallic) manganite systems.[34,35] In addtion, the Mn-O distance (Fig. 6) is that of metallic systems and the Mn-Mn/Mn-O-Mn peak recovers a shape reminescent of the high-temperature spectra.

Indirect measurements of charge order melting can be used to place these results into a broader context. The phase

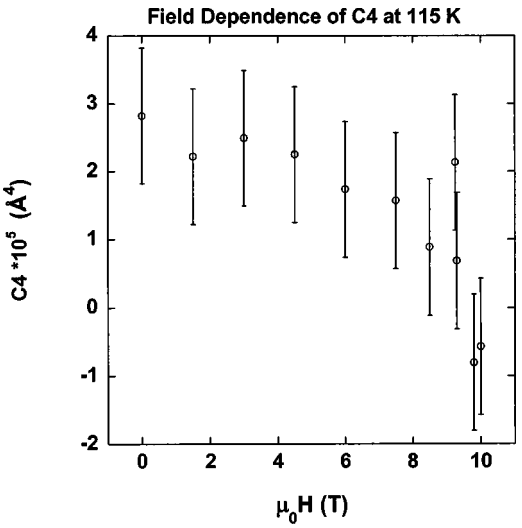

FIG. 5. The field-dependent fourth cumulant ($C4 = \langle (R - \langle R \rangle)^4 \rangle - 3\,\sigma^4$) for Mn-O bond. This quantity measures the flatness (kurtosis) of the radial distribution. At high field C4 vanishes indicating the disappearance of the Jahn Teller distortion [resulting in a narrow Gaussian distribution of distances (see Fig. 4)].

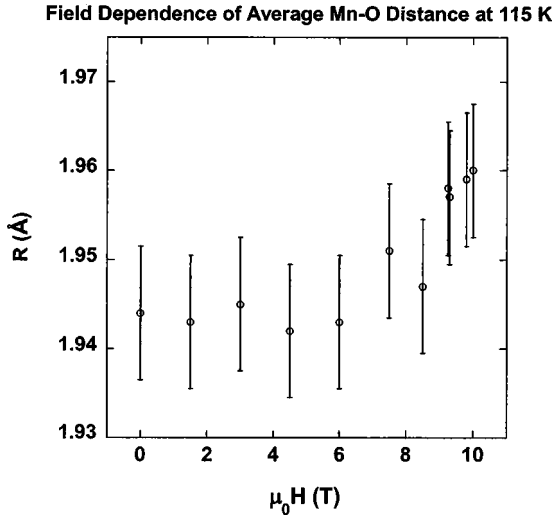

FIG. 6. The average Mn-O bond distance is seen to approach 1.96 Å, the value measured in the optimally ferromagnetic region of the $La_{1-x}Ca_xMnO_3$ phase diagram near $x=0.33$.

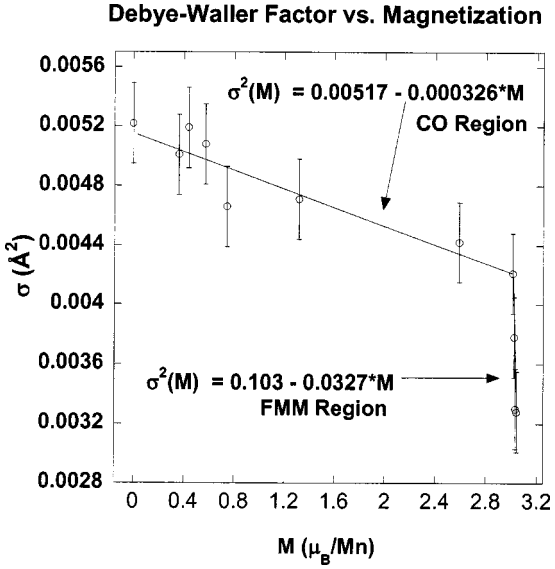

FIG. 7. Debye-Waller factor plotted as a function of magnetization. The JT distortion varies linearly in both the metallic (FMM) and charge-ordered (CO) regions. The rate of change of the JT distortion is 100 times faster after crossing into the ferromagnetic metallic region.

diagrams for the $R_{1/2}Ca_{1/2}MnO_3$ system with R =La, Pr, Nd, and Sm was examined in detail by Respaud *et al.*[7,12] based on isothermal magnetization measurements in pulsed magnetic fields up to 50 T. The fields required to melt the CO state at low temperature increases with the degree of the JT distortion and the tolerance factor $[t=d(R\text{-}O)/\sqrt{2}d(\text{Mn-O})]$ and inversely with the Mn-O-Mn bond angle. Hence, the farther away the Mn-O-Mn bond distance is from 180° the higher the field required to collapse the CO state. This is due to the fact that the Mn-Mn overlap via the O atom is weakened resulting in reduced double exchange interactions.

Support for this can be found in the fact that the substrate strain, which reduces the local JT distortion and increases the Mn-O-Mn bond angle, suppresses the field required to melt the CO state. This has been observed in $Pr_{1/2}Ca_{1/2}MnO_3$ films where the field required to melt the CO state at 100 K changes from ~20 T for bulk samples[12] to ~7 T for thin films[14] on $SrTiO_3$. More dramatic effects are found in the case of films of $Nd_{1/2}Sr_{1/2}MnO_3$ on $LaAlO_3$ where an optimal thickness (between 1500 and 2000 Å) is reached where the CO state is completely suppressed.[36] Detailed x-ray diffraction and x-ray absorption studies of this system showed that in the 2000 Å metallic films, the substrate induced strain reduced the local JT distortions—increasing the Mn-O-Mn bond angle[37] and destabilizing the CO state. Furthermore, the application of pressures (up ~3 GPa) is found to enhance the Mn-O-Mn bond angles leading to lower resistivity and higher metal insulator transition temperatures in the general charge ordered and metallic systems (see Refs. 38–40, and references therein). Pressures above ~3 GPa buckle the Mn-O-Mn bond angle enhancing the JT distortion of the MnO_6 octahedra leading to lower T_c and MI transition temperatures.

Hence the metal insulator transition temperature depends strongly on the starting Mn-O-Mn bond angle. The further away one is from 180° the higher the required melting fields. The concept generalizes to CO systems at higher dopings. Some critical magnetic field will fully align the Mn moments leading to a reduction in resistivity from reduced spin scattering. Further increases then significantly reduce the local JT distortion of the MnO_6 octahedra in the now ferromagnetic system.

IV. SUMMARY

The local structure about the Mn site in the half-doped system $La_{1/2}Ca_{1/2}MnO_3$ was measured in magnetic fields up 10 T to probe the melting of the charge-ordered state. The Debye-Waller factor for the first shell Mn-O distribution is reduced by ~40% between 0 and 10 T. Examination of the Mn-O and Mn-Mn correlations reveal three distinct regions in the structure-field diagram—a broad region with weak field dependence [mainly antiferromagnetic phase below 7.5 T (CO region)], a narrow-mixed phase region near ~8.5 T followed by a ferromagnetic phase region (FMM) with strong field-structure coupling. In terms of the magnetization, the variance of the Mn-O distribution is linear both in the CO and FMM regions with a 100-fold increase in slope in the FMM region. At high field the Mn-O radial distribution becomes Gaussian and the Mn-Mn correlations are enhanced—consistent with the dominance of a ferromagnetic phase. Comparison of the structural measurements with transport and magnetization measurements suggests that the exponential changes in resistivity in the first region are dominated by the reordering of the moments on the Mn sites from CE type antiferromagnetic to ferromagnetic order with only a weak change in the local distortions of the MnO_6 octahedra. The reduction in resistivity at high field is possibly the result of the delocalization of JT trapped electrons as the magnetic field destabilizes the local distortions.

ACKNOWLEDGMENTS

Data acquisition was performed at Brookhaven National Laboratory's National Synchrotron Light Source (NSLS) which is funded by the U. S. Department of Energy. The magnet acquistion funded by NSF IMR Grant No. DMR-0083189 and operational costs were funded by Grant No. NSF DMR-0209243. Sample preparation was supported by Maryland/Rutgers MRSEC NSF-DMR-0080008 (S-W.C.). We are indebted to S. Lamarra of NSLS for much technical assistance in the commissioning of the magnet.

*Present address: Department of Electrical and Computer Engineering, Northeastern University, Boston, MA 02115, USA.

[1] M. B. Salamon and M. Jaime, Rev. Mod. Phys. **73**, 583 (2001); Y. Tokura and Y. Tomioka, J. Magn. Magn. Mater. **200**, 1 (1999); J. M. D. Coey, M. Viret, and S. von Molnar, Adv. Phys. **48**, 167 (1999); M. Imada, A. Fujimori, and Y. Tokura, Rev. Mod. Phys. **70**, 1039 (1998); A. P. Ramirez, J. Phys.: Condens. Matter **9**, 8171 (1997); C. N. R. Rao and A. K. Cheetham, Adv. Mater. (Weinheim, Ger.) **9**, 1009 (1997).

[2] P. Schiffer, A. P. Ramirez, W. Bao, and S-W. Cheong, Phys. Rev. Lett. **75**, 3336 (1995).

[3] N. F. Mott, *Metal-Insulator Transitions* (Taylor and Francis, London, 1974); T. V. Ramakrishnan, J. Phys. C **111**, 4 (1994); P. P. Edwards and C. N. R. Rao, *The Metallic and Nonmetallic States of Matter* (Taylor and Francis, London, 1985); A. K. Raychaudhuri, Adv. Phys., **44**, 21 (1995); H. C. Nguyen and J. B. Goodenough, Phys. Rev. B **52**, 8776 (1995).

[4] A. J. Millis, Nature (London) **392**, 147 (1998).

[5] G. Xiao, E. J. McNiff, G. Q. Gong, A. Gupta, C. L. Canedy, and J. Z. Sun, Phys. Rev. B **54**, 6073 (1996); G. Xiao, G. Q. Gong, C. L. Canedy, E. J. McNiff, and A. Gupta, J. Appl. Phys. **81**, 5324 (1997).

[6] H. Kuwahara, Y. Tomioka, A. Asamitsu, Y. Moritomo, and Y. Tokura, Science **270**, 961 (1995); Y. Tomioka, A. Asamitsu, Y. Moritomo, H. Kuwahara, and Y. Tokura, Phys. Rev. Lett. **74**, 5108 (1995); M. Tokunaga, N. Miura, Y. Tomioka, and Y. Tokura, Physica B **246-247**, 491 (1998); M. Tokunaga, N. Miura, Y. Tomioka, and Y. Tokura, Phys. Rev. B **57**, 5259 (1998); M. Tokunaga, N. Miura, Y. Tomioka, and Y. Tokura, Phys. Rev. B **60**, 6219 (1999).

[7] M. Respaud, J. M. Broto, H. Rakoto, M. Goiran, A. Llobet, C. Frontera, J. L. Gracia Munoz, and J. Vanacken, J. Magn. Magn. Mater. **211**, 128 (2000); J. L. Gracia Munoz, M. Respaud, C. Frontera, A. Llobet, J. M. Broto, H. Rakoto, and M. Goiran, J. Appl. Phys. **85**, 5570 (1999).

[8] M. Roy, J. F. Mitchell, A. P. Ramirez, and P. Schiffer, Phys. Rev. B **58**, 5185 (1998); M. Roy, J. F. Mitchell, S. J. Potashink, and P. Schiffer, J. Magn. Magn. Mater. **218**, 191 (2000).

[9] V. N. Smolyaninova, A. Biswas, X. Zhang, K. H. Kim, B.-G. Kim, S. W. Cheong, and R. L. Greene, Phys. Rev. B **62**, R6093 (2000).

[10] J. Dho, I. Kim, and S. Lee, Phys. Rev. B **60**, 14 545 (1999).

[11] R. Mahendiran, M. R. Ibarra, A. Maignan, F. Millange, A. Arulraj, R. Mahesh, B. Raveau, and C. N. R. Rao, Phys. Rev. Lett. **82**, 2191 (1999).

[12] M. Respaud, A. Llobet, C. Frontera, C. Ritter, J. M. Broto, H. Rakoto, M. Goiran, and J. L. García-Muñoz, Phys. Rev. B **61**, 9014 (2000).

[13] Yu. F. Popov, A. M. Kadomtseva, G. P. Vorob'ev, K. I. Kamilov, Ya. S. Shtofich, V. Yu. Ivanov, A. A. Mukhin, and A. M. Balbashov, Phys. Solid State **45**, 1280 (2003).

[14] W. Prellier, A. M. Haghiri-Gosnet, B. Mercey, Ph. Lecoeur, M. Hervieu, Ch. Simon, and B. Raveau, Appl. Phys. Lett. **77**, 1023 (2000); W. Prellier, Ch. Simon, A. M. Haghiri-Gosnet, B. Mercey, and B. Raveau, Phys. Rev. B **62**, R16 337 (2000).

[15] A. Maignan, F. Damay, C. Martin, and B. Raveau, Mater. Res. Bull. **32**, 965 (1997).

[16] Q. Huang, J. W. Lynn, R. W. Erwin, A. Santoro, D. C. Dender, V. N. Smolyaninova, K. Gosh, and R. L. Greene, Phys. Rev. B **61**, 8895 (2000).

[17] P. G. Radaelli, D. E. Cox, M. Marezio, and S-W. Cheong, Phys. Rev. B **55**, 3015 (1997).

[18] G. Killias, M. Pissas, and A. Hoser, Physica B **276-278**, 778 (2000).

[19] A. Moreo, S. Yunoki, and E. Dagotto, Science **283**, 2034 (1999).

[20] N. Mathur and P. Littlewood, Phys. Today **56**, 25 (2003); J. C. Loudon, N. D. Mathur, and P. A. Midgey, Nature (London) **420**, 797 (2002).

[21] C. H. Booth, F. Bridges, G. H. Kwei, J. M. Lawrence, A. L. Cornelius, and J. J. Neumeier, Phys. Rev. Lett. **80**, 853 (1998); C. Meneghini, R. Cimino, S. Pascarelli, S. Mobilio, C. Raghu, and D. D. Sarma, Phys. Rev. B **56**, 3520 (1997); T. A. Tyson, J. Mustre de Leon, S. D. Conradson, A. R. Bishop, J. J. Neumeier, H. Röder, and Jun Zang, Phys. Rev. B **53**, 13 985 (1996).

[22] P. Schiffer, A. P. Ramirez, W. Bao, and S.-W. Cheong, Phys. Rev. Lett. **75**, 3336 (1995).

[23] P. G. Radaelli, D. E. Cox, M. Marezio, S.-W. Cheong, P. E. Schiffer, and A. P. Ramirez, Phys. Rev. Lett. **75**, 4488 (1995).

[24] For more details see URL www site http://eies.njit.edu/~tyson/Supmagnet.html

[25] *X-Ray Absorption: Principles, Applications, Techniques of EXAFS, SEXAFS and XANES*, edited by D. C. Konningsberger and R. Prins (Wiley, New York, 1988); P. A. Lee, P. H. Citrin, P. Eisenberger, and B. M. Kincaid, Rev. Mod. Phys. **53**, 679 (1981).

[26] The x-ray fine structure extraction was performed with the program ATHENA [B. Ravel (unpublished)].

[27] Fits of the R-Space Data to models was done using WINXAS™. See T. Ressler, J. Synchrotron Radiat. **5**, 118 (1998); T. Ressler, S. L. Brock, J. Wong, and S. L. Suib, J. Phys. Chem. B **103**, 6407 (1999).

[28] The FEFF7 code was used to generate the theoretical XAFS spectra. See A. L. Ankudinov and J. J. Rehr, Phys. Rev. B **56**, R1712 (1997).

[29] P. G. Radaelli, D. E. Cox, M. Marezio, and S.-W. Cheong, Phys. Rev. B **55**, 3015 (1997).

[30] P. Fornasini, F. Monti, and A. Sanson, J. Synchrotron Radiat. **8**, 1214 (2001); G. Dalba, P. Fornasini, and F. Rocca, Phys. Rev. B

47, 8502 (1993), and reference therein.
[31] E. A. Stern, Phys. Rev. B **48**, 9825 (1993).
[32] K. R. Poeppelmeier, M. E. Leonowicz, J. C. Scanlon, J. M. Longo, and W. B. Yelon, J. Solid State Chem. **45**, 71 (1982).
[33] J. Blasco, J. García, J. M. de Teresa, M. R. Ibarra, J. Perez, P. A. Algarabel, C. Marquina, and C. Ritter, Phys. Rev. B **55**, 8905 (1997).
[34] D. Cao, F. Bridges, C. H. Booth, and J. J. Neumeier, Phys. Rev. B **62**, 8954 (2000).
[35] C. Castellano, F. Cordero, R. Cantelli, C. Meneghini, S. Mobilio, D. D. Sarma, and M. Ferretti, Int. J. Mod. Phys. B **14**, 2725 (2000); C Meneghini, C. Castellano, A. Kumar, S. Ray, D. D. Sarma, and S. Mobilio, Phys. Status Solidi B **215**, 647 (1999).
[36] W. Prellier, A. Biswas, M. Rajeswari, T. Venkatesan, and R. L. Greene, Appl. Phys. Lett. **75**, 397 (1999).
[37] Q. Qian, T. A. Tyson, C.-C. Kao, W. Prellier, J. Bai, A. Biswas, and R. L. Greene, Phys. Rev. B **63**, 224424 (2001).
[38] C. Cui, T. A. Tyson, Z. Zhong, J. P. Carlo, and Y. Qin, Phys. Rev. B **67**, 104107 (2003).
[39] C. Cui and T. A. Tyson, Appl. Phys. Lett. **83**, 2856 (2003).
[40] C. Cui, T. A. Tyson, Z. Chen, and Z. Zhong, Phys. Rev. B **68**, 214417 (2003); C. Cui and T. A. Tyson, Appl. Phys. Lett. **84**, 942 (2004).